

Ion Energy Measurements in Mesh Assisted Plasma Immersion Ion Implantation

Scott Y. ALLAN, Christophe P. CORNET, David R. McKENZIE and Marcela M. M. BILEK

Applied and Plasma Physics, The School of Physics, The University of Sydney, NSW 2006, Australia

(Received: 1 September 2008 / Accepted: 18 December 2008)

Plasma immersion ion implantation (PIII) is a surface modification technique where an object whose surface is to be modified is placed in a plasma and pulse biased. For the treatment of insulators, a conductive mesh is often used to minimise the effects of surface charging. In this paper, ion energy distributions (IEDs) during mesh assisted PIII are studied experimentally, using a retarding field energy analyser (RFEA) and by a two dimensional (r,z) numerical simulation. The majority of ions originate from above the mesh top and mesh corners. Increasing pulse amplitude and/or mesh height increases the total ion flux. The IEDs measured at the centre of the target are made up of a low, medium and high energy peak. The high energy peak is caused by ions originating from above the mesh top. The low energy peak is caused by a potential hump formed inside the mesh. The medium energy peak is caused by ions entering from the sheath above the mesh corners. The analyser only discriminates ions based on the z component of their velocity and so records an increase in ion energy of the medium energy peak as the mesh height increases.

Keywords: plasma immersion ion implantation, ion energy distribution, mesh, retarding field energy analyser, numerical simulation

1. Introduction

Since its introduction in the 1980s [1] plasma immersion ion implantation (PIII) has become a widely used technique for the surface modification of materials. In the basic PIII process, negative voltage pulses (up to 150 kV) are applied to a target immersed in a plasma. These pulses, with periods of between one to several hundred microseconds, accelerate plasma ions into the target. Compared to conventional beamline ion implantation, the main advantage of PIII is that it allows complex shaped objects to be treated quickly without the need for target manipulation or complicated ion beam sources [2].

PIII has been used in the treatment of a variety of materials. For example, metal surfaces treated with PIII show improved resistance to wear and corrosion [3]. PIII has also been used to modify the electrical and optical properties of semiconductors [4] and the wettability and adhesive properties of polymers [5, 6]. For insulators, to minimise the effects of surface charging and improve the depth of modifications, a conductive mesh can be placed above the insulator and pulse biased [7–9].

The energy distribution of ions arriving at the target determines the extent of surface modifications. Due to the large voltages and short timescales involved, there have been limited experimental measurements of the ion energy distribution (IED) during PIII. These measurements have involved the use of a Faraday cup type device to measure ion current [10–12] or theoretical methods based on depth profile measurements [13, 14]. In mesh assisted PIII, investigation of IEDs has been limited to computer simulation studies [15, 16].

In this paper, the factors affecting the IED during mesh

assisted PIII are investigated experimentally and with simulation. Pulse amplitudes in the -50 to -500 V range were used which have applications in areas such as the treatment of polymers [17] and the deposition of diamond like carbon films [18]. The effects of pulse amplitude and mesh height on IEDs during PIII were studied using a retarding field energy analyser (RFEA). To better explain the structure of the IEDs, a two dimensional numerical simulation of ion trajectories in the plasma sheath and mesh regions was also carried out.

2. Experimental Method

The experimental setup used is shown in Fig. 1. Measurements were carried out in a capacitive 13.56 MHz radio frequency (RF) argon plasma at a pressure of 5 mTorr. The RF electrode was disc shaped with a diameter of 13 cm

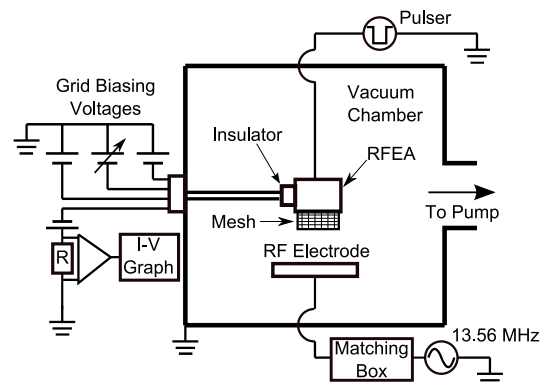


Fig. 1 Schematic of the experimental setup used for time-resolved ion energy measurements during PIII using a retarding field energy analyser (RFEA).

author's e-mail: sallan@physics.usyd.edu.au

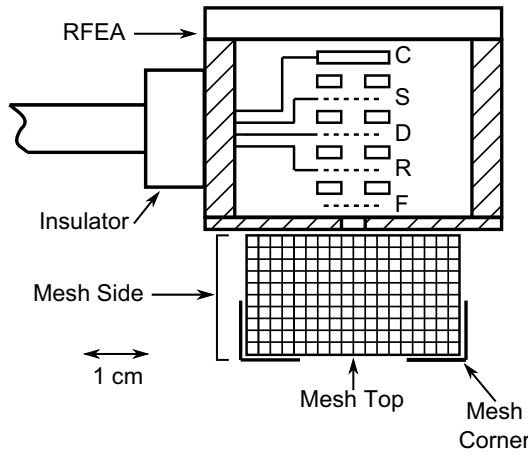


Fig. 2 Cutaway diagram of the RFEA with a cylindrical mesh fitted over the entrance aperture. The grids and spacers inside the RFEA are not drawn to scale. The first grid (F) is connected to the probe body. The second grid (R) is biased negatively to repel electrons. The voltage on the third grid (D) is swept upwards to discriminate which ions are allowed to pass. The fourth grid (S) is biased negatively to minimise secondary electron emissions from the collector (C) where ion current is measured. The plasma enters through a 4 mm diameter orifice at the centre of the RFEA front.

and the vacuum chamber was cylindrical with a diameter of 44 cm and length of 46 cm.

Time resolved ion energy measurements were performed using a four grid retarding field energy analyser (RFEA) with an outer body that could be pulse biased up to -500 V. A cutaway diagram of the RFEA is shown in Fig. 2. The grids and insulating spacers inside the RFEA are not drawn to scale. The analyser discriminates ions based on the z component of their velocity and is cylindrical with a diameter of 50 mm, length of 40 mm and has an inlet orifice with a diameter of 4 mm. The nickel grids used in the RFEA were approximately $5 \mu\text{m}$ in thickness and had square holes with widths of $39.4 \mu\text{m}$ and an open area of sixty percent. Teflon spacers with a thickness of approximately 0.8 mm were used to insulate the grids from each other. The first grid of the analyser (F) is connected to the probe outer body and covers the inlet orifice to prevent electric fields from inside the analyser disturbing the plasma. The second grid (R) is biased negatively to repel electrons and the third grid (D), called the discriminator, has a voltage that is swept upwards to discriminate ions according to their energy. The fourth grid (S) is biased negatively to minimise the effects of secondary electron emission at the negatively biased collector (C) where ion current is measured. The overall distance from the front of the analyser to the collector is approximately 3.5 mm.

Stainless steel mesh with 1mm square holes and a transparency of sixty nine percent was used to make cylinders with a diameter of 36 mm which were attached to the analyser front. The analyser inlet orifice was in the centre

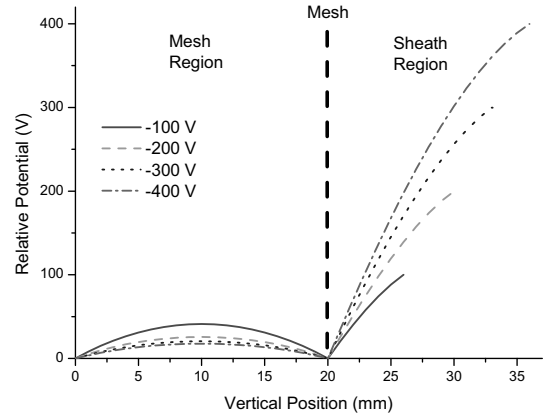


Fig. 3 Simulation results for the relative potential (actual potential - potential on mesh) versus vertical distance (z) along the centre line ($r=0$) through a 2 cm high mesh for different potentials on the mesh.

of the base of the mesh. For a typical measurement, the analyser body and mesh were pulse biased and the ion current recorded as a function of time for each discriminator voltage using a TDS2024 oscilloscope with a time resolution of one microsecond. This allowed ion current versus discriminator voltage graphs to be constructed for different times during the pulse on and pulse off periods. The IED is proportional to the negative of the first derivative of the ion current versus discriminator voltage data [19].

3. Simulation Method

A two dimensional numerical simulation in cylindrical (r,z) coordinates was used to study the trajectories and energies of ions in the sheath and mesh regions. The potential values were determined by using the relaxation method to solve Poisson's equation, taking into account the decrease in ion density as the ions accelerate. The electron density was assumed to be zero. Above the planar regions of the mesh, the sheath thickness was set to the one dimensional Child Law sheath thickness (s) [20]:

$$s = \frac{\sqrt{2}}{3} \left(\frac{\epsilon_0 T_e}{en_0} \right)^{\frac{1}{2}} \left(\frac{2V_0}{T_e} \right)^{\frac{3}{4}} \quad (1)$$

where T_e is the electron temperature (set to 3 eV), n_0 is the plasma density (set to $1 \times 10^{15} \text{ m}^{-3}$), e is the charge on an electron and V_0 is the sheath potential. Around the mesh corners, the sheath thickness is less than the Child Law value [21]. In the mesh corner regions a linear interpolation of the sheath thickness was made between the one dimensional Child Law value and a value of seventy percent of the Child Law value at the bisector of the corner. A graph of the relative potential (actual potential - potential on mesh) versus vertical distance (z) along the centre line ($r=0$) through a 2 cm high mesh is shown in Fig. 3. The potential inside the mesh is greatest for an applied voltage of -100 V as ions are moving at their slowest.

In the simulation, ions were started at the sheath edge with the Bohm velocity and trajectories perpendicular to the sheath edge. IEDs were constructed using ions which reached the collector inside the analyser which was positioned in the centre of the mesh 4 mm below the analyser front. The relative peak heights in the IEDs may not be correct due to the assumption that all ions enter the sheath at the Bohm velocity. In a real plasma, ions can enter the sheath at speeds greater than the Bohm velocity and this would act to spread the peaks in the IEDs. A Monte Carlo approach was used to model hard sphere collisions between ions and neutrals using a velocity independent collision cross section based on the argon atom radius.

4. Results

In the first experiments a 2 cm high mesh was attached to the RFEA and pulse biased at -300 V with a 1.25 kHz square wave with a pulse on time of 200 μ s. Fig. 4 shows the IEDs obtained 190 μ s after the start of the pulse when different sections of the mesh were covered. The location of the covered mesh sections are as shown in Fig. 2. A high energy peak at 310 eV is observed for all IEDs except for the top covered mesh. This high energy peak corresponds to ions which did not collide and gained the maximum potential of the pulse amplitude plus the time averaged plasma potential. The plasma potential oscillates on a timescale much faster than the time taken by an ion to cross the sheath [22] so that ions will only experience the time averaged plasma potential. The number of maximum energy ions is only slightly affected by covering the mesh sides or corners. A medium energy peak at 175 eV is also observed. This peak decreases in size when the mesh sides are covered and disappeared when a 1 cm section around the mesh corners was covered. A low energy peak close to zero energy, observed when the mesh sides were covered is believed to be low energy ions trapped by the covered side walls and the potential hump observed inside the mesh in Fig. 3. When the mesh cylinder top is covered almost no ions are measured.

Fig. 5 shows the simulation results for the origins of the components of the IED obtained for a -300 V pulse applied to a 2 cm high cylindrical mesh and the RFEA at a pressure of 5 mTorr. The high energy peak at 309 eV is due to uncollided ions from the mesh top that reach the probe collector. The peak position is slightly larger than 300 eV due to the finite time step size used in the simulations. The majority of ions from the sheath sections above the mesh corners which reach the probe collector do not collide and form a medium energy peak at 200 eV. While these ions have both an r and z component to their velocities, the analyser only discriminates ions based on the z component of their velocity. In PIII, it is the z component which determines the depth of surface modifications. Ions from the top and corner sheath sections with energies less than these peaks represent ions which have undergone

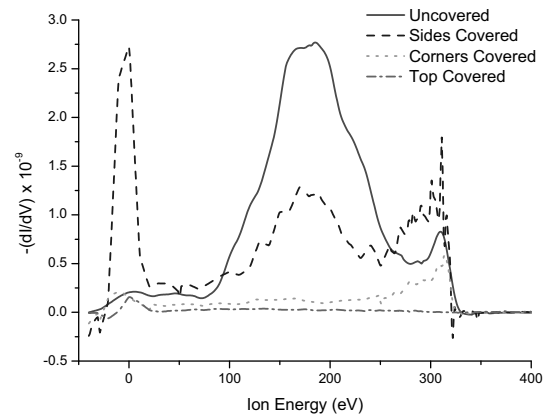


Fig. 4 IEDs obtained when different sections of a 2 cm high mesh were covered during PIII with a -300 V pulse with a frequency of 1.25 kHz and pulse on time of 200 μ s. The location of the covered mesh sections are as shown in Fig. 2. IEDs were obtained 190 μ s after the start of the pulse.

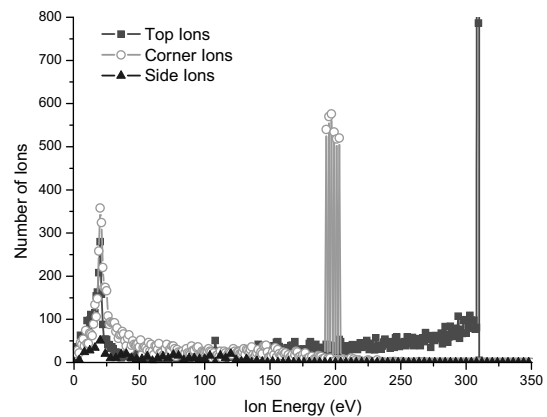


Fig. 5 Simulation results showing the components of the IED obtained for a -300 V pulse applied to a 2 cm high cylindrical mesh and the RFEA at a pressure of 5 mTorr.

collisions in the sheath and/or mesh regions. The low energy peak at 20 eV is due to ions which collided inside the mesh on the probe side of the 20 V potential hump shown in Fig. 3. Ions from the side sections of the mesh do not contribute significantly to the IED. These results help explain the origins of the high, medium and low energy peaks in Fig. 4. The high energy peak is caused by ions from directly above the analyser inlet, the medium energy peak are ions from above the mesh corners and the low energy peak is caused by the potential hump formed inside the mesh.

The effects of pulse amplitude on the IED were investigated using a 2 cm high mesh and pulses with a frequency of 1.25 kHz and a pulse on time of 200 μ s. The IEDs obtained 190 μ s after the pulse switched on are shown in Fig 6. For each IED, a high energy peak was observed at an energy representing the pulse amplitude plus the time averaged plasma potential. As the pulse amplitude increases, the area under the curves increases indicating an increase

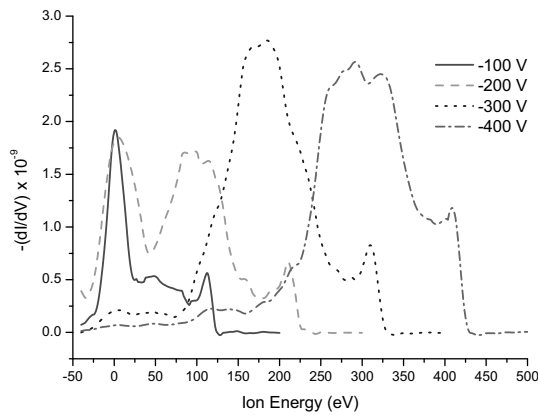


Fig. 6 IEDs obtained 190 μ s after the pulse switched on for different pulse amplitudes with a 2 cm high mesh and pulses with a frequency of 1.25 kHz and pulse on period of 200 μ s.

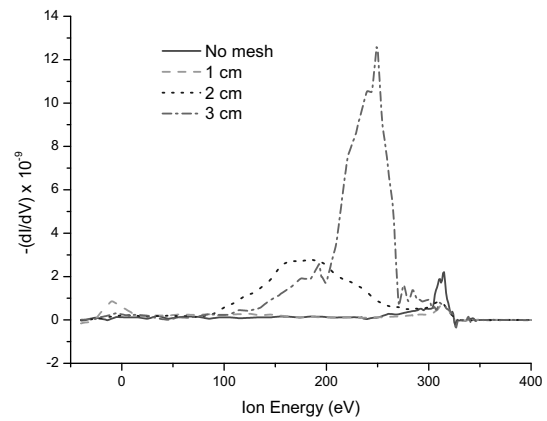


Fig. 8 IEDs obtained 190 μ s after the pulse switched on for various mesh heights with a -300 V pulse with a frequency of 1.25 kHz and a pulse on time of 200 μ s.

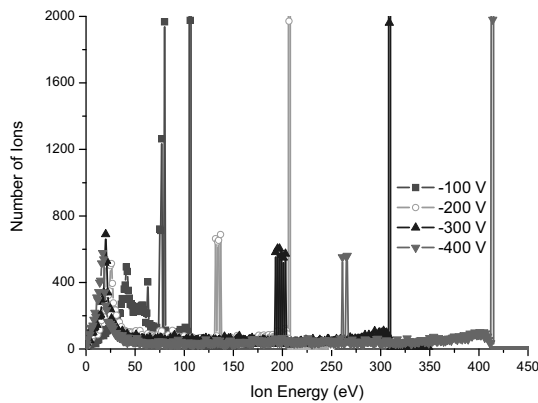


Fig. 7 Simulation results showing the effects of pulse amplitude on the IEDs obtained using a 2 cm high cylindrical mesh at a pressure of 5 mTorr.

in ion flux. This is caused by an increase in the surface area of the plasma-sheath boundary as the sheath width increases with pulse amplitude. For the -200, -300 and -400 V IEDs, medium energy peaks occur at 98, 175 and 298 eV respectively. Low energy peaks are also observed close to 0 eV for both the -100 and -200 V IEDs. The low energy peaks are believed to be caused by ions which have collided and are trapped by the potential hump inside the mesh seen in Fig. 3. The relative height of this potential hump is more significant for the -100 and -200 V pulses and affects their IEDs more than for the -300 and -400 V IEDs.

Fig. 7 shows the simulation results for the effects of pulse amplitude on the IED for a 2 cm high cylindrical mesh at a pressure of 5 mTorr. For each amplitude, high energy peaks are seen close to the pulse amplitude energy. These represent uncollided ions from the sheath above the top section of mesh. Additional medium energy peaks are observed at 77, 134, 197 and 264 eV for the -100, -200, -300 and -400 V IEDs respectively. These represent uncollided ions which originated from the sheath sections above

the mesh corners. While these ions have both a r and z component to their velocities the analyser only discriminates the ions based on the z component of their velocities. The low energy peaks formed between 0 and 65 eV represent ions which collided on the probe side of the potential hump inside the mesh region. These results help explain the IED structure seen in Fig. 6. The high energy peaks are caused by ions from directly above the analyser inlet, the medium energy peaks are caused by ions from above the mesh corners and the low energy peaks are caused by ions trapped by the potential hump inside the mesh. The broad structure of the -100 V IED in Fig. 6 appears to be due to the large height of the potential hump inside the mesh region.

The effects of mesh height were investigated for a -300 V pulse with a frequency of 1.25 kHz and a pulse on time of 200 μ s. The IEDs obtained for cylindrical meshes of various heights 190 μ s after the pulse switched on are shown in Fig. 8. A high energy peak at 312 eV due to ions which experienced the full sheath potential plus the time averaged plasma potential is observed for all mesh heights. For the 2 and 3 cm meshes, medium energy peaks are also observed at approximately 175 and 250 eV respectively. These peaks are not seen in the IEDs for the 1 cm and no mesh results. As the mesh height increases, the total area under the IEDs increases due to a larger ion flux. This is caused by the increase in the surface area of the plasma-sheath boundary with increasing mesh height.

Fig. 9 shows the simulation results for the effects of mesh height on the IEDs obtained for a -300 V pulse at a pressure of 5 mTorr. For all mesh heights, a high energy peak is seen close to 305 eV which is caused by uncollided ions originating from the sheath section directly above the probe inlet aperture. For the 2 and 3 cm IEDs, medium energy peaks are observed at 197 and 260 eV respectively. These peaks are caused by uncollided ions which originated from the sheath regions above the mesh corners. As the mesh height increases, the z component of the velocity

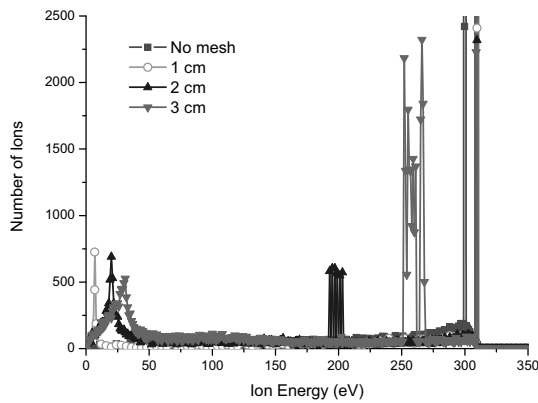


Fig. 9 Simulation results showing the effects of mesh height on the IEDs obtained for a -300 V pulse at a pressure of 5 mTorr.

of the ions reaching the collector from the sheath above the mesh corners becomes larger, shifting the medium energy peak to a higher energy. For the 1 cm mesh, ions from the sheath above the mesh corners are beyond the acceptance angle of the collector and are not measured. This is similar to the experimental results in Fig. 8 which show no medium energy peak for the 1 cm mesh and no mesh IEDs.

5. Conclusion

In mesh assisted PIII, the majority of ions originate from the sheath sections above the mesh top and corners. The IEDs obtained at the base of the centre of a mesh during PIII showed a low, medium and high energy peak. The high energy peak is caused by ions from directly above the mesh. The low energy peak is caused by the potential hump formed inside the mesh. The medium energy peak is caused by ions from above the mesh corners. The analyser used only discriminates ions based on the z component of their velocity. As the mesh height increases, the z component of the velocity of the medium energy peak ions increases, shifting the medium energy peak to a higher energy. As pulse amplitude and/or mesh height increases, the total ion flux increases due to the increase in the surface area of the plasma-sheath boundary.

- [1] J. R. Conrad, J. L. Radtke, R. A. Dodd, F. J. Worzala and N. Tran, *J. Appl. Phys.* **62**, 4591 (1987).
- [2] A. Anders, *Handbook of Plasma Immersion Ion Implantation and Deposition* (John Wiley and Sons, New York, 2000) p. 244.
- [3] Y. Chang and D. Wang, *Surf. Coat. Technol.* **200**, 2187 (2005).
- [4] Rajkumer, M. Kumar, P. J. George, S. Mukherjee and K. S. Chari, *Surf. Coat. Technol.* **156**, 253 (2002).
- [5] Y. Kim, Y. Lee, S. Han and K. Kim, *Surf. Coat. Technol.* **200**, 4763 (2006).
- [6] J. H. Hong, Y. Lee, S. Han and K. Kim, *Surf. Coat. Technol.* **201**, 197 (2006).
- [7] R. K. Y. Fu, X. Tian and P. K. Chu, *Rev. Sci. Instrum.* **74**, 3697 (2003).
- [8] R. K. Y. Fu, P. K. Chu and X. Tian, *J. Appl. Phys.* **95**, 3319

- (2004).
- [9] A. Kondyurin, B. K. Gan, M. M. M. Bilek, K. Mizuno and D. R. McKenzie, *Nucl. Instr. and Meth. in Phys. Res. B* **251**, 413 (2006).
- [10] S. Mändl, J. Brutscher, R. Günzel and W. Möller, *Surf. Coat. Technol.* **93**, 234 (1997).
- [11] T. Ikehata, K. Shioya, N. Y. Sato and K. Yukimura, *Surf. Coat. Technol.* **186**, 209 (2004).
- [12] P. L. Kellerman, J. D. Bernstein and M. P. Bradley, *Conference on Ion Implantation Technology 2000*, 484 (2000).
- [13] S. Qin, C. Chan and N. E. McGruer, *Plasma Sources Sci. Technol.* **1**, 1 (1992).
- [14] N. P. Barradas, A. J. H. Maas, S. Mändl and R. Günzel, *J. Appl. Phys.* **81**, 6642 (1997).
- [15] R. C. Powles, D. T. K. Kwok, D. R. McKenzie and M. M. Bilek, *Phys. Plasmas* **12**, 0935071 (2005).
- [16] Y. Cho, H. June Lee, C. Park, H. Lee and S. Lee, *J. Appl. Phys.* **100**, 123303 (2006).
- [17] E. V. Barnat, T. -M. Lu and J. Little, *J. Appl. Phys.* **90**, 4946 (2001).
- [18] F. Thiéry, C. Vallée, Y. Arnal and J. Pelletier, *Surf. Coat. Technol.* **186**, 146 (2004).
- [19] I. H. Hutchinson, *Principles of Plasma Diagnostics* (Cambridge University Press, Sydney, 1987) p. 83.
- [20] M. A. Lieberman, A. J. Lichtenberg, *Principles of Plasma Discharges and Materials Processing* (John Wiley and Sons, New York, 1994) p. 165.
- [21] C. Donolato, *J. Phys. D:Appl. Phys.* **38**, 397 (2005).
- [22] E. Kawamura, V. Vahedi, M. A. Lieberman and C. K. Birdsall, *Plasma. Sources Sci. Technol.* **8**, R45 (1999).